Chitinase-like protein promotes tumorigenesis through disruption of cell polarity via enlarged vesicles.

Dilan Khalili[1], Martin Kunc[1], Sarah Herbrich[1], Anna M. Müller[1] and Ulrich Theopold[1]

[1] Department of Molecular Biosciences, The Wenner-Gren Institute (MBW), Stockholm University, 10691 Stockholm, Sweden

Ulrich Theopold, Department of Molecular Biosciences, The Wenner-Gren Institute (MBW), Stockholm University, Svante Arrheniusväg 20c, 10691 Stockholm, Sweden

Phone: +46-8-164181

Email: uli.theopold@su.se

Abstract:

Chitinase-like proteins (CLPs) are associated with tissue-remodelling and inflammation but also with several disorders, including fibrosis, atherosclerosis, allergies, and cancer. However, the CLP's role in tumors is far from clear. Here, we utilize *Drosophila melanogaster* to investigate the function of CLPs (imaginal disc growth factors; Idgf's) in Ras^{V12} dysplastic salivary glands (SGs). We find one of the Idgf's members, *Idgf3,* to be transcriptionally induced in a tissue- and cell-autonomously manner in a *Drosophila* hypertrophic model for early tumor progression. Induction involves non-canonical JNK-signaling via a positive feedback loop mediated by reactive oxygen species (ROS). Moreover, Idgf3 accumulates in enlarged vesicles (EnVs) that promote tumor progression by disrupting cytoskeletal organization, independent of Rab5 and Rab11. The process is mediated via Rac1 and the downstream component, αSpectrin, which localizes to the EnVs. Similar to Idgf3, expression of two human members of the CLP family in *Drosophila* SGs aggravates tumor-related phenotypes. Our data provide new insight into a phylogenetically conserved tissue-autonomous CLP function in tumors and identify specific targets for tumor control.

Introduction:

Chitinase-like protein (CLPs), including human Ch3L2 (YKL-39) and Ch3L1 (YKL-40) are released in various inflammatory conditions, including tumors. These proteins are secreted amongst others by immune cells, are often associated with a poor prognosis, and may promote tumor growth through interaction with the tumor microenvironment (Roslind and Johansen 2009, Shao, Hamel et al. 2009). CLPs are upregulated in patients with ductal tumors, including tumors in the lung, the breast and the pancreas (Johansen, Jensen et al. 2006, Uhlen, Zhang et al. 2017).

The discovery of the human Rat sarcoma (Ras) oncogene more than 40 years ago has led to a substantial improvement of our understanding of cancer biology. The oncogene is mutated or dysregulated in a large number of non-physiological contexts, including pancreatitis

(Fernandez-Medarde, De Las Rivas et al. 2021). Pancreatitis is characterized by inflammation, death-signaling, fibrosis, loss of cell polarity, immune cell recruitment, and obstruction of pancreatic ducts mediated via *KRAS* (Pinho, Chantrill et al. 2014). However, the causal connection between CLPs' function and tumor progression is only partially elucidated (Park, Yun et al. 2020).

Animal models have been increasingly used in molecular oncology. This includes the fruitfly *Drosophila melanogaster*, where overexpression of dominant-active Ras (Ras^{V12}) in proliferating tissue leads to benign tumors, simultaneous reduction of cell polarity genes and to progression towards an invasive stage. (Brumby and Richardson 2003, Pagliarini and Xu 2003, Igaki, Pagliarini et al. 2006, Perez, Lindblad et al. 2017). Central to this switch is the C-Jun N-terminal kinase (JNK) - signaling pathway, which can become activated via loss of cell polarity and promotes tumor growth (Zhu, Xin et al. 2010). However, the outcome of activated JNK is mediated in a context-dependent manner due to downstream effects, several of which are yet to be elucidated (Ciapponi, Jackson et al. 2001, Zeke, Misheva et al. 2016). Among potential JNK regulators, spectrin family members belong to cytoskeletal proteins which form a spectrin-based membrane skeleton (SBMS) (Bennett and Baines 2001). Through the Rac family of small GTPases, cell polarity and SBMS organization are maintained (Lee and Thomas 2011, Fletcher, Elbediwy et al. 2015). Although the exact relationship between Spectrin and JNK in tumors remains to be established, Rac1 cooperates with JNK in tissue growth (Baek, Kwon et al. 2010, Wertheimer, Gutierrez-Uzquiza et al. 2012, Archibald, Mihai et al. 2015).

To explore the tissue autonomous function of CLPs in a ductal tumor, we utilize the *Drosophila melanogaster* salivary glands (SGs) - like the pancreas a terminally differentiated secretory organ. Generally, *Drosophila* CLPs are endogenously expressed in the larvae and include six members, termed Idgf 1-6 (Imaginal disc growth factors), which are involved in wound healing and restoration of cell organization (Kirkpatrick, Matico et al. 1995, Kawamura, Shibata et al. 1999, Kucerova, Kubrak et al. 2016, Yadav and Eleftherianos 2018). The SGs epithelial luminal organization and the conserved activation of the tumor-promoting signaling factors make them suitable for dissecting CLP's tissue autonomous function. Moreover, the lumen separating a single layer of cells can be disrupted by constitutive active *Drosophila Ras* (Ras^{V12}) (Krautz, Khalili et al. 2020).

Here we investigated the role of *Drosophila* Idgf's in Ras^{V12} SGs. We show that one of the CLP's members, *Idgf3*, is induced cell-autonomously, leading to a partial loss of epithelial polarity and decrease of the SG lumen. This involves induction of non-canonical JNK-signaling that regulates *Idgf3* independently of the downstream transcription factor Jun and Fos. Instead, ROS production via JNK promotes induction of *Idgf3*, creating a tumor-promoting signaling loop. Idgf3 through Rac1 promotes the formation of enlarged vesicles (EnVs) via αSpectrin. Inhibiting EnV formation by knocking-down *Idgf3* and the downstream factor, *αSpectrin,* restores cell organization. Similar to Idgf3, overexpression of two human CLPs in Drosophila Ras^{V12} SGs, aggravates hyperplasia and leads to EnV formation for one human CLP. Thus, our work signifies the evolutionary conserved importance of tumor-induced CLP's in the cell-autonomous dysregulation of ductal organs.

Results

Idgf3 promotes a dysplastic phenotype

Obstruction of the SG lumen by the constitutive-active oncogene, Ras^{V12}, under the *Beadex-Gal4* driver (denoted as Ras^{V12}) disrupts organ function between 96 h and 120 h after egg desposition (AED) (Khalili, Kalcher et al. 2021). Being that CLPs have been implicated in the loss of cell polarity (Morera, Steinhauser et al. 2019), we investigated whether *Drosophila* CLPs contribute to this phenotype. In order to find out whether CLPs were induced in Ras^{V12} glands, we assessed relative mRNA levels at two different time points, 96 h and 120h AED. Only one of the *CLP* members, namely *Idgf3,* was significantly upregulated at both time points (Fig. 1B and Fig. S1A). Therefore, we decided to focus on *Idgf3's* effects on dysplastic glands.

To characterize the spatial and temporal expression of *Idgf3* we performed in situ hybridization (ISH) using Idgf3-*specific* probes. In SGs of w^{1118} *(*denoted as *WT)* larvae, *Idgf3* was expressed in the most proximal part (PP) confirming earlier results (Fig. S1B at 96 h, (Kawamura, Shibata et al. 1999)). In line with qPCR data (Fig. S1A), a higher level of *Idgf3* was detected in Ras^{V12} SGs (Fig. S1C). At 120 h, we still observed *Idgf3* in the PP of *WT* glands, while in Ras^{V12} larvae, the signal was again substantially stronger and detected throughout the whole gland (Fig. S1D-E).

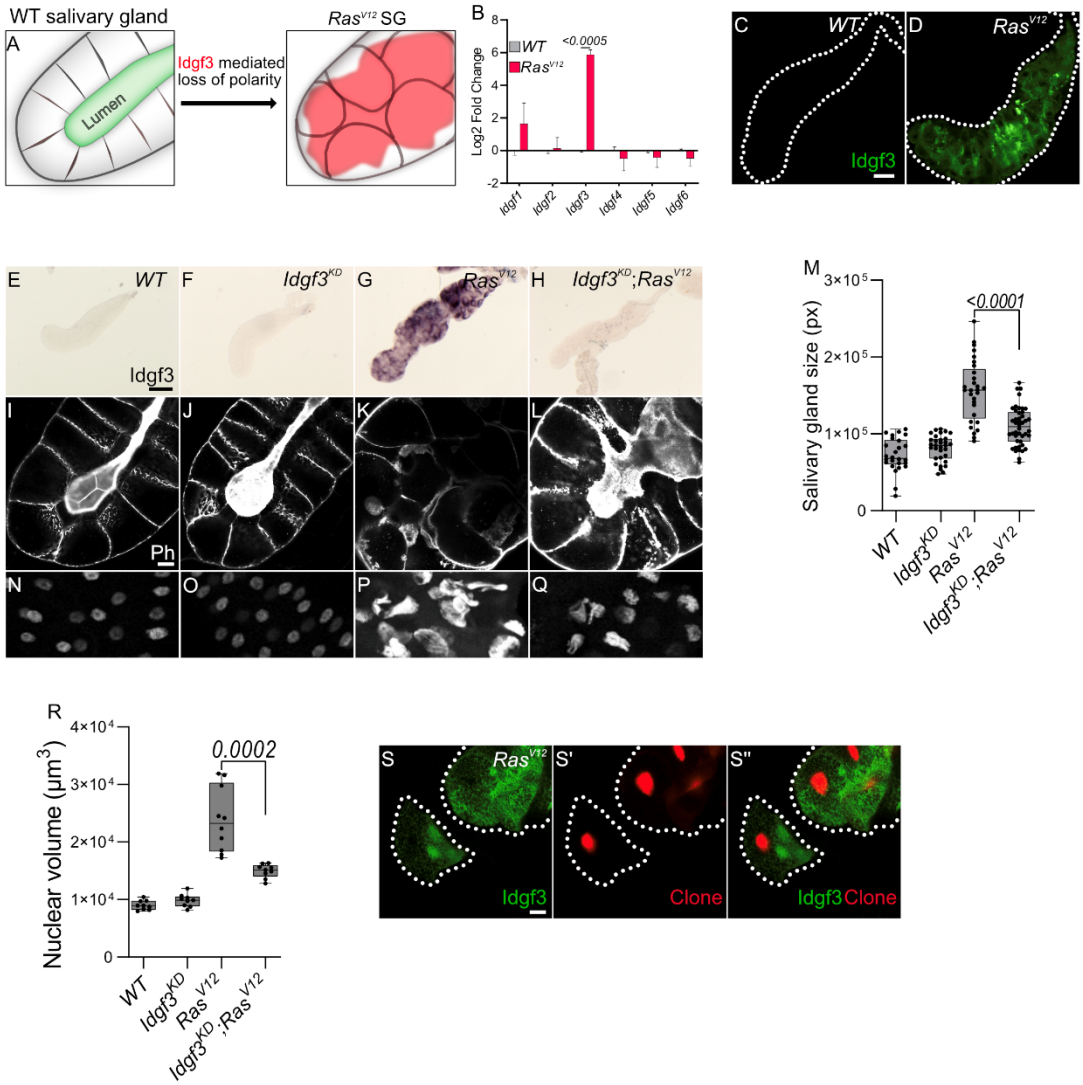

Figure 1 Idgf3 promotes growth and disrupts tissue architecture in a cell-autonomous manner

(A) Idfg3 drives dysplasia upon oncogene, *Ras^{V12}*, overexpression.
(B) qPCR data showing induction of *Idgf3* in 120 h AED *Ras^{V12}* glands.
(C-D) Idgf3 tagged with GFP was localized in the dysplastic glands.
(E-H) Knock-down of *Idgf3* in *Ras^{V12}* glands confirmed reduced mRNA levels as shown with in situ hybridization.
(I-L) F-actin (Phalloidin) staining revealed partial restoration of the lumen in *Idgf3-KD;Ras^{V12}* glands, in comparison to *Ras^{V12}* alone.
(M) SG size quantification showing a reduction in tissue size in *Idgf3-KD;Ras^{V12}* SG compared to *Ras^{V12}* alone.
(N-Q) Nuclei in DAPI stained SG displayed a reduced size in *Idgf3-KD;Ras^{V12}*.
(R) Nuclear quantification showing nuclear volume in the indicated genotypes.
(S-S'') SG *Ras^{V12}*clones displaying strong Idgf3::GFP signal.
Scale bars in (C-D) represent 100 μm (E-H), 0.3 mm and (I-L, S-S'') 20 μm. Data in (B) represent 3 independent replicas summarized as mean ± SD. Boxplot in (M) represent at least 20 SG pairs and (R) represent 10 SG pairs. Whisker length min to max, bar represent median. P-value quantified with Student's t-test.

Idgf3 contains an N-terminal signal peptide and has been detected in hemolymph (Karlsson, Korayem et al. 2004). To analyze its subcellular tissue distribution in SGs, we used a C-terminally GFP-tagged version of Idgf3 (Kucerova, Kubrak et al. 2016). At 96 h we could not detect Idgf3 in the whole *WT* or Ras^{V12} animals (Fig. S1F-G'), possibly due to limited sensitivity. Likewise, 120 h old *WT* larvae did not show any detectable signal (Fig. S1H-H') while a strong Idgf3 signal was detected in Ras^{V12} SGs (FigS1I-I'). To better understand Idgf3 distribution at a higher resolution, we dissected 120 h AED glands. *WT* glands had a weaker Idgf3::GFP signal in comparison to the Ras^{V12} (Fig. 1C-D). Moreover, Idgf3 was unevenly distributed throughout Ras^{V12} SGs (Fig. 1D).

The increased level of *Idgf3* between 96 h and 120 h strongly correlated with loss of tissue- and cell-organization and an increased nuclear volume. In order to characterize the role of Idgf3 in Ras^{V12} glands, we used a specific *Idgf3 RNA-interference* (*RNAi*, denoted as *KD*). We focused on 120 h larvae, unless otherwise stated, since they showed the most robust dysplastic phenotype. Efficient knockdown of *Idgf3* was confirmed using ISH and at protein level (Fig 1E-H, S1J-M; quantified in N, (Kucerova, Kubrak et al. 2016)). Macroscopic inspection showed that *Idgf-KD;*Ras^{V12} SGs were smaller than Ras^{V12} SGs (Fig 1G-H, quantified in Fig 1M), thus resembling WT controls. To gain insight into the cellular organization, we stained the glands for F-actin (Phalloidin: Ph) and DNA using DAPI. In *Idgf-KD* the cells retained their cuboidal structure, and the lumen was visible as in *WT*, indicating that Idgf3 on its own does not affect cellular architecture (Fig. 1I-J). In contrast, in Ras^{V12} glands cellular architecture was lost, and the lumen was absent (Fig. 1K, (Khalili, Kalcher et al. 2021). In *Idgf-KD;*Ras^{V12} SGs a reversal to the normal distribution of F-actin and partial restoration of the lumen was observed (Fig 1 L). Similarly, the nuclear volume, which increased in Ras^{V12} SGs returned to near wild type levels upon *Idgf3-KD* (Fig. 1 N-Q, quantified in Fig 1R). This indicates that *Idgf3-KD* can rescue Ras^{V12}-induced dysplasia.

In order to unravel the specific effects mediated by Idgf3 we further investigated Ras^{V12} associated phenotypes, including fibrosis and the cellular immune response. As recently reported, Ras^{V12} SGs displayed increased levels of the extracellular matrix components (ECM), including collagen IV and SPARC (BM40, (Khalili, Kalcher et al. 2021)). *Idgf-KD* alone did not affect SPARC levels in comparison to the *WT* (Fig. S1 O-P) but *Idgf-KD;*Ras^{V12} SGs displayed significantly reduced SPARC levels in comparison to Ras^{V12} (Fig. S1 Q-R, quantified in S). To assess whether this led to a reduced inflammatory responses, we examined the recruitment of plasmatocytes, macrophage-like cells previously reported to be recruited towards tumors (Perez, Lindblad et al. 2017). We found that both control and *Idgf-KD* glands did not show recruitment of hemocytes (Fig. S1T-U). In contrast to the effects on ECM components, *Idgf3-KD* in Ras^{V12} glands did not lead to any changes in hemocyte attachment (Fig. S1V-W, quantified in X).

Finally, to assess whether Idgf3::GFP was induced cell-autonomously, we generated clones expressing Ras^{V12} and nuclear *red fluoresent protein* (*RFP*) through a *heat-shock* driver. We found that Idgf3::GFP was expressed in the clonal tumor cells, whereas the WT cells were devoided of Idgf3::GFP (Fig. 1 S).

Taken together, upon Ras^{V12} overexpression, *Idgf3* is induced cell-autonomously and promotes SG overgrowth, loss of cell organization, and fibrotic-like accumulation of the ECM, but not immune cell recruitment.

Idgf3 induces dysplasia via a non-canonical JNK-pathway

Dysplasia is driven by internal and external factors that work either in concert or independently. Similar to what we observed in *Idgf3-KD;*Ras^{V12} glands, blocking the sole *Drosophila* JNK member *basket* reverts several tumour phenotypes. Moreover, the dysplastic loss of apical and basolateral polarity between 96 h and 120 h is driven by the JNK-pathway (Fig. 2A, (Krautz, Khalili et al. 2020)). The time frame in which we observed upregulation of *Idgf3* coincided with the period during which blocked JNK restored tissue organization and homeostasis, similar to what occurs in *Idgf-KD;*Ras^{V12} SGs (Fig. 1L, S1R). Therefore, we sought to determine the role of JNK-signaling in the regulation of Idgf3.

First, we performed a targeted JNK RNAi-screen using Idgf3::GFP intensity in the glands as a readout for KD of JNK signaling components. We confirmed the sensitivity of the Idgf3::GFP construct by *Idgf3-KD* in Ras^{V12} SGs compared to Ras^{V12} glands (Fig. S2A-B, quantified in Fig S2L). KD of the two classical TNF receptors upstream of JNK, *Grnd* (*Grindelwald*) and *Wgn* (*Wengen*) similarly reduced Idgf3::GFP intensity (Fig 2C-D, quantified in F, S2A-L; for the complete screen, (Palmerini, Monzani et al. 2021)). A similar effect was observed upon suppression of *dTAK,* a downstream component of Grnd/Wgn, in Ras^{V12} glands (Fig S2A, E, quantified in L). Furthermore, suppressing JNK using a dominant-negative version (JNK^{DN}) displayed the strongest reduction of the Idgf3::GFP signal (Fig 2SA, F, quantified in L). Similar effects were observed with *JNK-KD* (Fig. 2B, E, quantified in F). In contrast suppression of the two transcription factors that form the AP1 complex downstream of JNK using dominant-negative variants Jun (Jun^{DN}) and Fos (Fos^{DN}) (Perkins, Dailey et al. 1988) did not have any effect (Fig. S2I-J, quantified in L). In agreement, Jun^{DN} and Fos^{DN} did not reduce phospho-JNK (pJNK) levels, although Fos^{DN} reduced the activity of the JNK-reporter construct to some extent (TRE.GFP, Fig. S2M-R', quantified in S and T). Altogether this suggests that Idgf3 protein levels are regulated downstream of JNK either independently of transcriptional regulation through JUN/FOS or in a redundant manner.

To further characterize Idgf3 regulation, we asked whether the reduction of Idgf3::GFP intensity was due to transcriptional regulation. ISH revealed a substantial reduction of endogenous *Idgf3* transcript levels in JNK^{KD};Ras^{V12} (Fig. 2G-H) glands, and a weaker signal in JNK^{DN};;Ras^{V12} (Fig. S2U-X) SGs, which was also confirmed using qPCR (Fig. S2Y).

Having observed that *Idgf3* transcript levels were not affected by *Grnd-KD* or *Wgn-KD* (Fig. 2G-I), we further investigated their involvement in activation of the JNK pathway in SGs. Using an anti-JNK phosphorylation antibody and the JNK reporter construct as readouts, the signal was significantly reduced in *Grnd-KD* and *Wgn-KD*, in comparison to *WT* glands (Fig. 2K-M', quantified in Q, R). However, in contrast to Ras^{V12} SGs, *Grnd-KD* did not reduce pJNK signaling, and *Wgn-KD* led only to a slight reduction ($p < 0.029$, Fig. 2N-P', quantified in Q, R) (Kanda, Igaki et al. 2002, Andersen, Colombani et al. 2015). The TRE signal was not affected by either KD (Fig. 2D, F). We substantiated these data with qPCR, which confirmed efficient

KD of *Grnd* and *Wgn* in *Grnd-KD;Ras^{V12}* and *Wgn-KD;Ras^{V12}*, respectively. However, the levels of JNK target genes, Puc and MMP, were not affected. In line with the ISH, *Idgf3* levels did not change either (Fig. S2Z). Collectively, this suggests that in *Ras^{V12}* driven dysplastic glands, Grnd and Wgn do not activate the canonical JNK-pathway. Instead, they contribute to Idgf3 regulation at the post-transcriptional level. Several scenarios could explain these observations (i) disruption of the secretory machinery may inhibit canonical JNK activation (Palmerini, Monzani et al. 2021), (ii) an alternative JNK-activating signaling pathway may be activated by *Ras^{V12}* (Wu, Chen et al. 2015, Krautz, Khalili et al. 2020) or (iii) disruption of cell polarity prevents proper JNK signaling (Zhu, Xin et al. 2010).

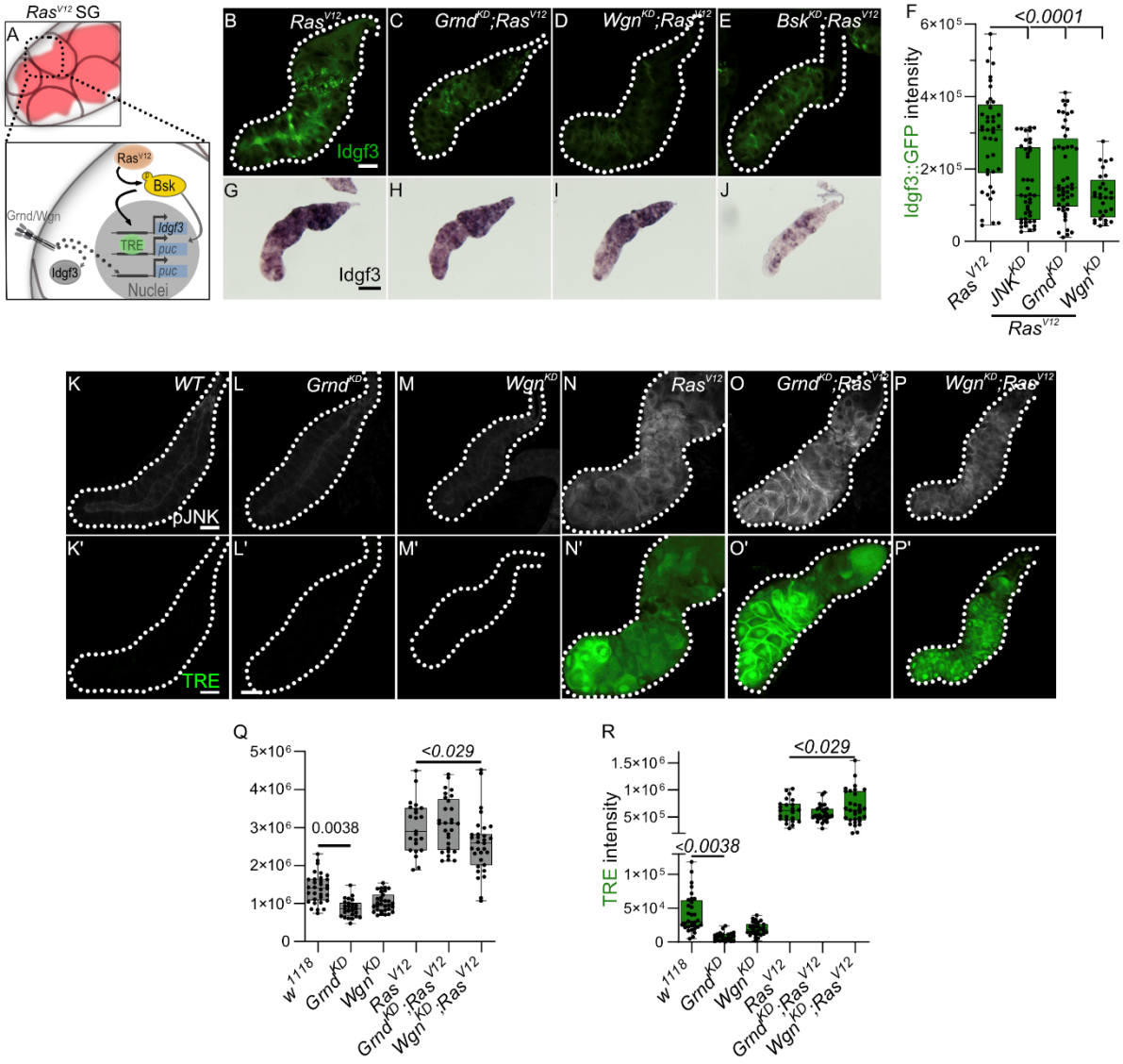

Figure 2 Idgf3 dysplasia is mediated through JNK activity

(A) Non-canonical JNK mediated *Idgf3* induction.

(B-E) Representative images of Idgf3::GFP in a JNK targeted screen (see Fig, S2 for the complete survey).

(F) Quantification showing Idgf3::GFP intensity was reduced by *Grnd-KD*, *Wgn-KD* and *JNK-KD* in *Ras^{V12}* SG.

(G-I) *In-situ hybridization* showing reduced transcript abundance for *Idgf3* in *JNK-KD;Ras^{V12}* SG.

(K-P') pJNK staining and TRE reporter construct showing non-canonical JNK signaling in *Ras^{V12}* SG.
(Q-R) pJNK and TRE intensity quantification indicating strong intensity in *Grnd-KD;Ras^{V1}* and *Wgn-KD;Ras^{V1}* glands.
Scale bars in (B-E, K-P') represent 100 μm and (G-I) 0.3 mm. Boxplot in (F,Q and R) represent at least 20 SG pairs. Whisker length min to max, bar represent median. P-value quantified with Student's t-test.

ROS promotes *Idgf3* induction via JNK

To further dissect Idgf3 regulation, we focused on the positive JNK regulators, reactive oxygen species (ROS) both intra- and extracellularly (Diwanji and Bergmann 2017, Perez, Lindblad et al. 2017). We previously reported that ROS production in *Ras^{V12}* SGs increases via JNK (Fig. 3A, (Krautz, Khalili et al. 2020)). To inhibit ROS intra- and extracellularly, we separately overexpressed the H_2O_2 scavengers Catalase (Cat) and a secreted form of Catalase, IRC (immune-regulated Catalase), and the O_2^- scavenger SODA (Superoxide dismutase A), in the *Ras^{V12}* background and quantified Idgf3::GFP intensity. Reducing levels of intracellular H_2O_2 (*Cat-OE*), but not O_2^- (*SODA-OE*) lowered Idgf3::GFP intensity (Fig. S3A-D, quantified in S3E). Similarly, reduction of extracellular H_2O_2 by the secreted version of Catalase lowered Idgf3::GFP levels (Fig. 3B-E, quantified in F). Similar to the reduced tissue size and improved tissue integrity in *Idgf3-KD;;Ras^{V12}* SGs, overexpression of *IRC* in *Ras^{V12}* SGs also reduced SG size (Fig. S3F), improved tissue integrity and restored the SG lumen (Fig. 3R-V). In order to discriminate Idgf3 post- and transcriptional regulation, we performed qPCR on *IRC-OE;Ras^{V12}* SGs and found a significantly lower level of *Idgf3* (Fig. 3K) in comparison to *Ras^{V12}*. The *Idgf3* reduction was only detectable in *IRC-OE;Ras^{V12}* glands since ISH on SGS detected similar levels of Idgf3 transcripts in *CatA-OE;Ras^{V12}* and *SodA-OE;Ras^{V12}* in comparison to *Ras^{V12}* SGs (Fig. 3G-J and S3G-L). Moreover, H_2O_2 affected JNK target gene expression, indicating a global regulation of JNK. This suggests that ROS, specifically H_2O_2, are involved in the activation of Idgf3 signaling and disruption of tissue integrity.

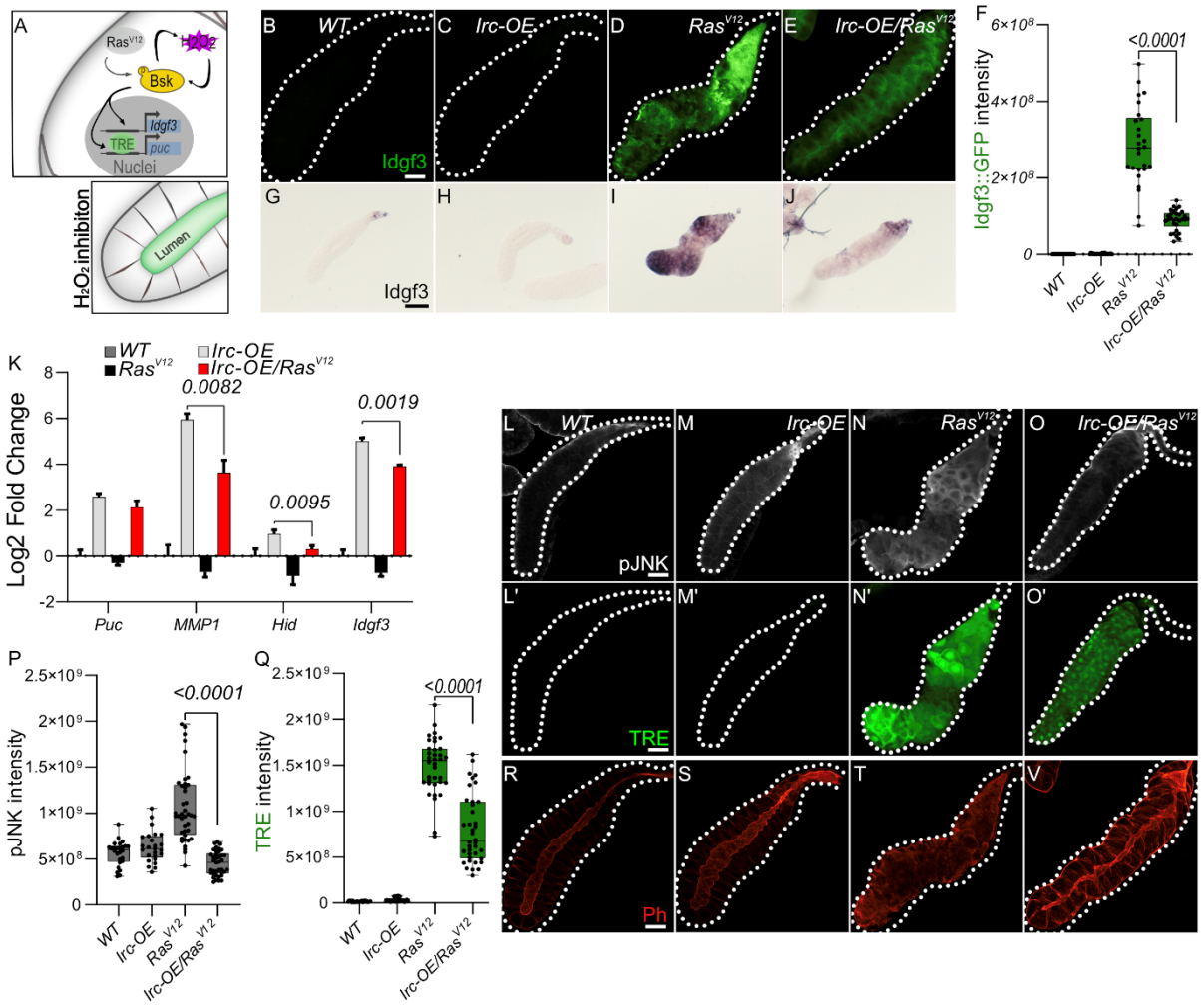

Figure 3 *Idgf3* regulation feeds into a JNK-ROS feedback loop

(A) H_2O_2, regulates *Idgf3* expression through JNK.

(B-E) Reduction of H_2O_2 by overexpression of secreted catalase (immune regulated catalase; IRC) lowered Idgf3::GFP levels (Quantified in F).

(G-J) ISH showing reduced expression of *Idgf3* in *IRC-OE;Ras^{V12}*glands.

(K) qPCR data showing reduction of *Idgf3, MMP1* and *Hid* in *IRC-OE;Ras^{V12}*glands.

(L-O') pJNK staining and TRE reporter constructs showing reduced intensity in *IRC-OE;Ras^{V12}* in comparison to *Ras^{V12}* glands, quantified in (P-Q).

(R-U) Phalloidin staining showing partially restored lumen in *IRC-OE;Ras^{V12}* glands.

Scale bars in (B-J, L-U) represent 100 μm. Data in (K) represent 3 independent replicas summarized as mean ± SD. Boxplot in (F,P-Q) represent at least 20 SG pairs. Whisker length min to max, bar represent median. P-value quantified with Student's t-test.

ROS mediates JNK activation through a positive feedback loop (Perez, Lindblad et al. 2017). Therefore we asked whether ROS induced *Idgf3* expression via the JNK-pathway. As done previously, we addressed pJNK and TRE.GFP levels. Interestingly, all tested ROS scavengers reduced pJNK levels (Fig. 3L-O, quantified in P, S3M-R, quantified in S) although TRE levels were not influenced in *SOD-OE;Ras^{V12}*, in contrast to *Cat-OE;Ras^{V12}* and *IRC-OE/Ras^{V12}* (Fig. 3L'-O', quantified in Q, S3M'-R', quantified in T). In summary, ROS contribute to the positive regulation of pJNK. In addition, overexpression of extracellular but not intracellular Catalase

reduces Idgf3 induction via JNK, indicating that *Idgf3* might be regulated via the secretory pathway. Duox and Nox, present in secretory glands, are transmembrane proteins that may generate extracellular ROS (Faria and Fortunato 2020). Their conserved function has been shown to facilitate tumor progression but whether they play an important role in Ras^{V12} SGs remains to be elucidated (Aggarwal, Tuli et al. 2019).

Idgf3 accumulates in enlarged vesicles

We previously noted the uneven distribution of Idgf3 in Ras^{V12} SGs (Fig. 1D). To further understand how Idgf3 promotes dysplasia, we dissected its subcellular localization in different areas of the SGs (Fig. 4A). We stained the glands for F-actin (Phalloidin) and addressed Idgf3::GFP localization at high resolution (Fig. 4B-C'). Interestingly, we observed Idgf3::GFP clusters surrounded by F-actin (Fig. 4C-C': arrow). Using a different salivary gland driver (*AB-Gal4*) to drive expression of Ras^{V12}, we also detected increased expression of Idgf3::GFP and localization within vesicle-like structures (Fig. S4A-B: arrow). The size of the vesicle-like structure was between 10-43 μm in comparison to secretory *Drosophila* vesicles (3-8μm, Fig. 4D, (Tran and Ten Hagen 2017)). We refer to these as enlarged vesicles (EnVs). Based on the increased Idgf3 levels, we wondered whether the protein was aggregating in EnVs.The aggregation marker, p62 (*Drosophila* Ref(2)P, (Bartlett, Isakson et al. 2011) detected signals throughout the cytoplasm of Ras^{V12} *SGs*. In contrast, EnVs did not display any signs of aggregated proteins (Fig. S4C-D').

Since we had observed a loss of secretion in Ras^{V12} *SGs* we next addressed the presence of EnVs within the secretory pathway. We overexpressed two versions of human phosphatidylserine binding protein, MFG-E8 (Milk fat globule-EGF factor), without (referred to as non-secreted: Fig .4F-F',I-I') and with a signal peptide (referred to as secreted: Fig. 4G-G',J-J', (Asano, Miwa et al. 2004)). In the controls, the non-secreted MFG-E8 was found in the cytoplasm, whereas the secreted version was detected in both the cytoplasm and in the lumen (Fig. 4F-G'). In Ras^{V12} SGs, the non-secreted form was surrounding the EnVs (arrow), indicating the presence of phosphatidylserine on their membrane (Fig. 4I-I'). In contrast, the secreted form localized to the EnVs (Fig. 4J-J': arrow). These data suggest that (1) EnVs are surrounded by a lipid membrane and (2) EnVs likely derive from the secretory pathway.

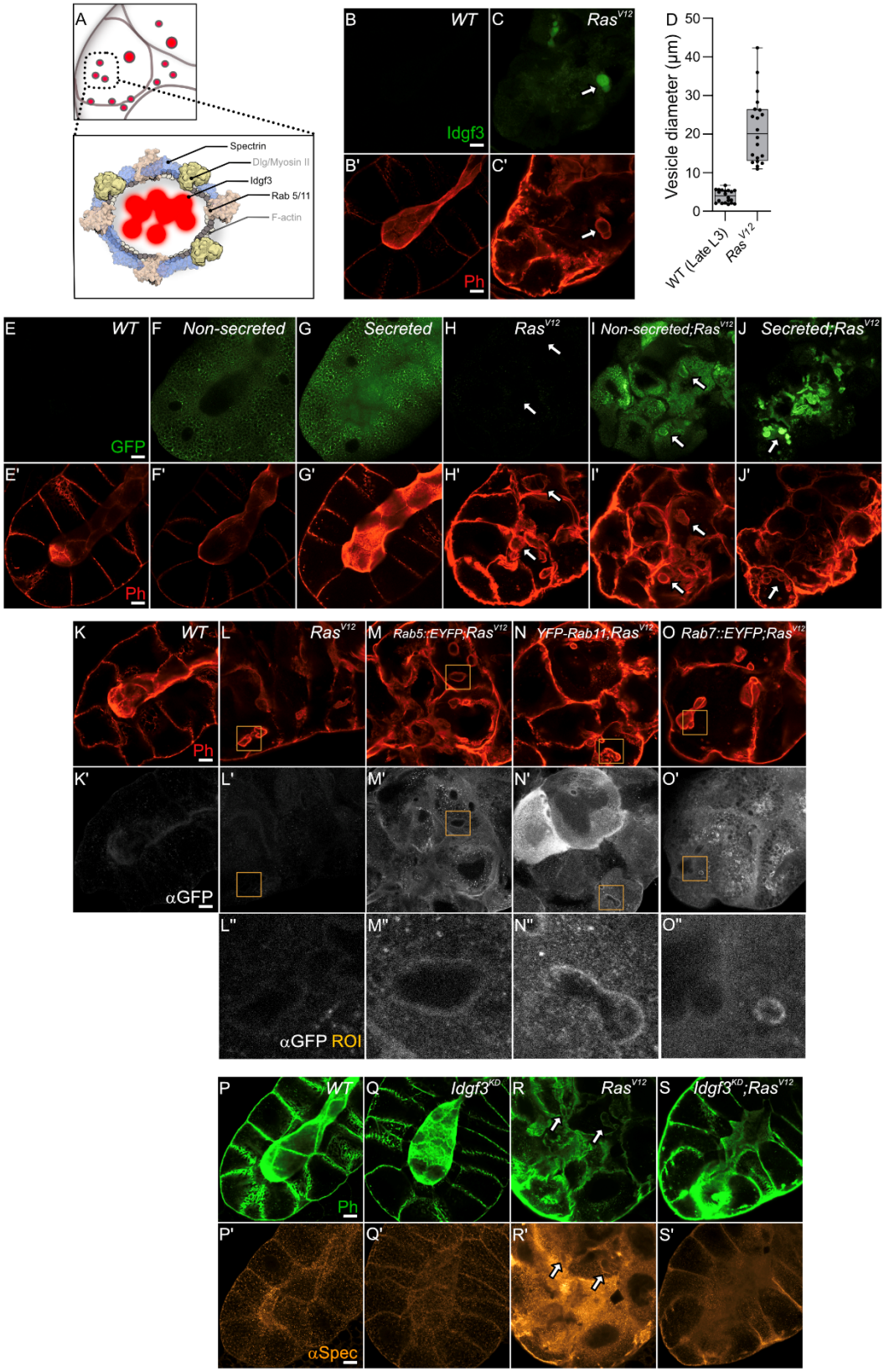

297

298 **Figure 4 *Idgf3* promotes formation of enlarged endosomes**

299 (A) Idgf3 enclosed by enlarged endosomes coated by cytoskeletal and cell polarity proteins.

300 (B-C') Idgf3::GFP clusters coated with Phalloidin.

301 (D) Vesicle size quantification showing *Ras^{V12}* enlarged vesicles in comparison to prepupae SG

302 vesicles.

(E-J') Non secreted MFGE8 localizes to the surface of EnVs, co-stained with phalloidin. The secreted MFGE8 is packaged into EnVs in *Ras^{V12}*glands.
(K-O'') Vesicle markers showing positively stained EnVs when detecting Rab5 and Rab11 but not Rab7.
(P-S') αSpectrin staining showing restoration of normal distribution in *Idgf3-KD;Ras^{V12}*glands. Scale bars in (B-C', E-J', K-O'' and P-S') represent 20 μm. Boxplot in (D) represent 20 EnVs. Whisker length min to max, bar represent median.

In order to further characterize Idgf3-positive EnVs we co-expressed vesicle-specific Rab's coupled with a GFP fluorophore, an autophagolysosomal marker (Atg8), an autophagy marker (Vps35), and a marker for phosphatidylinositol-3-phosphate-(PtdIns3P: *FYVE*)-containing endosomes in *Ras^{V12}* glands (For a complete set see Fig. S4I-Q"). To increase sensitivity, we stained with anti-GFP and co-stained with Phalloidin. Localization of Rabs and phalloidin to the same vesicles was observed with Rab5 and Rab11 but not Rab7 (Fig. 4K-O'). Moreover, the EnVs were also positive for PtdIns3P (Fig. S4P-P"). In line with their dependence on secretion, this potentially identifies EnVs as enlarged recycling endosomes. EnV accumulation in *Ras^{V12}* glands between 96 h and 120 h implies that (i) early endosome formation and fusion are either increased compared to *WT* or (ii) that recycling endosomes are not normally fused back to the apical membrane leading to their intracellular accumulation (Fig. S4E-H"). The latter hypothesis correlates with the loss of apico-basolateral polarity and the disruption of secretion due to a lack of a luminal structure ((Khalili, Kalcher et al. 2021) and Fig. S4E''-H"). To test the first hypothesis, we blocked the formation of early endosomes with *Rab5^{DN}*. Apico-basolateral polarity, detected by a visible lumen, was not affected by *Rab5^{DN}*. Moreover, *Rab5^{DN};Ras^{V12}* did not block EnV formation and restoration of apicobasal polarity (Fig. S4R-U: arrow). Halting the recycling endosome pathway via *Rab11^{DN}* increased endosome accumulation without affecting cell polarity (Fig. S4V: arrow). In contrast, in *Rab11^{DN};Ras^{V12}* SGs, endosomes were not accumulating, and EnVs were still detected (Fig. S4W).Taken together, EnV formation is independent of the classical recycling pathway, suggesting other candidates are involved in the generation of EnVs.

Idgf3 promotes loss of cell polarity via α-Spectrin positive enlarged endosomes

Spectrins, cytoskeletal proteins which form a cortical network, have been shown to also play a role in secretion, cellular homeostas and cell polarity (Tjota, Lee et al. 2011, Lattner, Leng et al. 2019) all of which were affected in *Ras^{V12}*-SGs (Khalili, Kalcher et al. 2021). Therefore, we stained for αSpectrin, one of the three members of the spectrin family (Williams, Smith et al. 2003) and found it to localize to the EnVs (Fig. 4SX-Y'''). Moreover, we found markers for cell polarity including Dlg and Myosin II to also co-localize with the EnVs (Fig. S4Z—AC': arrow). Finally, we asked whether Idgf3 in *Ras^{V12}* SGs was responsible for EnV formation and mislocalization of αSpectrin and found that indeed, *Idgf3-KD;Ras^{V12}* glands lacked EnVs, and αSpectrin distribution was partially restored (Fig 4Q-T').

Taken together, Idgf3 promotes EnV formation and disruption of cellular integrity, assessed by mislocalization of αSpectrin, Dlg and Myosin II.

Rac1 promotes the formation of EnVs via αSpectrin

In SGs, overexpression of Rac generates enlarged vesicles coated with Spectrin (Lee and Thomas 2011) with similarity to the EnVs described here. Therefore, we sought to investigate the role of the Rac1 pathway in Ras^{V12} glands (Fig. 5A). Supporting a role in dysplasia, Ras^{V12} glands stained with Rac1 showed a stronger staining in comparison to the control. Moreover, we observed Rac1 localized to EnVs (Fig. 5B-C'). To further assess Rac1's role in dysplasia we overexpressed *Rac1*. Surprisingly, *Rac1-OE* alone was sufficient to induce *Idgf3*, an effect that was not increased in *Rac1-OE*;Ras^{V12} (Fig. 5D-E, I-J). Due to the pleiotropic effects of the $Rac1^{DN}$ construct, we addressed Rac1 function by modulating the expression of the Rac1 effector molecule, *Pak* (Lee and Thomas 2011). *Pak-KD*;Ras^{V12} did not reduce *Idgf3* levels but improved the histology of the gland (Fig. 5I,K). Conversely, overexpression of Pak^{CA} did not increase *Idgf3* levels and had no detectable effect on F-actin distribution (Fig S5A-C''). In contrast, Rac1 activity via Pak does affect Ras^{V12} SG integrity: Idgf3::GFP levels were increased in *Rac1-OE* SGs and F-actin was disorganized (Fig. S5D-F'', quantified in I). However, the *Rac1-OE* glands did not grow larger compared to Ras^{V12}, indicating additional signals are necessary for gland overgrowth. Also, *Pak-KD*;Ras^{V12} SGs displayed a more regular F-actin distribution leading to restoration of the lumen and proper secretion of Idgf3 (Fig. S5G-H'').

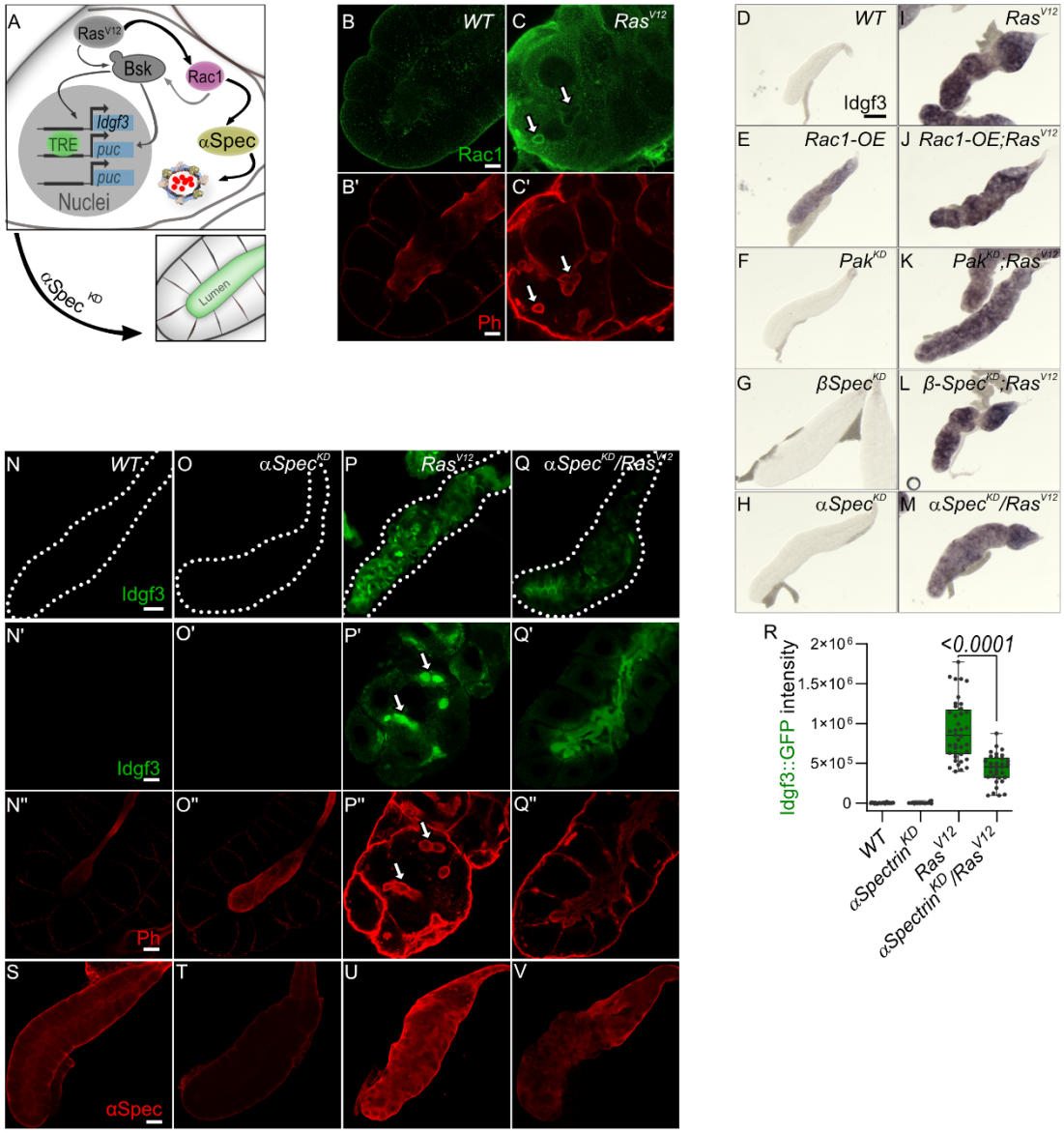

Figure 5 Rac1 promotes EnVs formation through αSpectrin?

(A) Redistribution of the spectrin-based membrane skeleton (SBMS) facilitates loss of cell polarity through Idgf3 packed EnVs.

(B-C') Rac1 staining showing EnVs co-localizing with Phalloidin.

(D-M) ISH showing increased *Idgf3* staining in *Rac1-OE* glands. Improved tissue structure in *Pak-KD;Ras^{V12}* and *αSpectrin*-KD/*Ras^{V12}* glands did not affect *Idgf3* expression in comparison to *Ras^{V12}*.

(N-V) Reduced levels of αSpectrin (αSpectrin-*KD* /*Ras^{V12}*) reduces Idgf3::GFP levels quantified in (R) prevents formation of EnVs and largely restores the SG lumen (arrows indicate EnVs). αSpectrin staining (S-V) is quantified in (S5V).

Scale bars in (B-C' and N'-Q'') represent 20 μm, (D-M) 0.3 mm and (N-Q and S-V) 100 μm. Boxplot in (R) represent at least 20 SG pairs. Whisker length min to max, bar represent median. P-value quantified with Student's t-test.

To further characterize the Rac1 pathway, we asked whether the downstream components *β-Spec* and *αSpec* affected *Idgf3* transcript levels in *Ras^{V12}* glands. I*dgf3*-specific ISH of *β-Spec-KD;Ras^{V12}* or *αSpec-KD*/*Ras^{V12}* showed that this was not the case. However, SG histology

improved in *αSpec-KD/Ras^{V12}* (Fig 5I, L-M). Therefore, we further looked into *αSpec-KD/Ras^{V12}* and its effect on F-actin organization and noted a similar effect as in *Pak-KD;Ras^{V12}* (Fig 5N-Q'), namely that Idgf3::GFP levels were reduced. However, most of the Idgf3::GFP signal was detectable in the lumen (Fig. 5Q-Q', quantified in R). The ISH was substantiated with qPCR which showed increased levels of *Idgf3* in *Rac1-OE*, slightly increased levels in *Pak^{CA}*, whereas *αSpec-KD/Ras^{V12}* showed a slight reduction (Fig. S5J). Moreover, JNK target genes, such as *Puc* and *Grnd* were upregulated in *Rac1-OE* and to some extent in *Pak^{CA}* (Fig. S5J). Supporting regulation of JNK target genes via JNK, *Rac1-OE* showed higher TRE level compared to *Pak^{CA}* (Fig. S5K-M'', quantified in N and O). Interestingly, *αSpec-KD/Ras^{V12}* reduced JNK and TRE levels (Fig S5P-S, quantified in T and U) without affecting JNK target genes (Fig. S5J). In summary, *Rac1-OE* was sufficient to induce *Idgf3* in salivary glands. However, in *Ras^{V12}* SGs, additional signals contribute to *Idgf3* regulation. This is most likely due to additional effectors feeding into JNK signaling. Our data suggest, downregulation and upregulation of the JNK pathway may have different outcomes at the transcriptional and post-transcriptional level. Nevertheless, αSpectrin promotes EnV formation in *Ras^{V12}* SGs, disrupts polarity, proper secretion, and localization of Idgf3.

JNK promotes EnV formation via Idgf3 upstream of αSpectrin

The data presented here suggest that Idgf3 promotes EnV formation (Fig. 4R-S). Moreover, this likely occurs post-transcriptionally (Fig. S6A) since *Idgf3-KD;Ras^{V12}* did not lead to reduced expression of *aSpectrin*. In contrast, at 96 hours, overexpression of Idgf3 throughout the whole gland, as shown by ISH (Fig. S6B-E), led to an increase in the number of glands with endosomes (Fig. S6F-I''', quantified in J). The observed activation of αSpec via Idgf3 prompted us to investigate the epistasis between JNK, Idgf3, Rac1, and αSpec. First, we addressed epistasis between Idgf3 and JNK since blocking JNK function by expressing a dominant-negative form (*Bsk^{DN}*) resulted in restoration of apical-basal polarity (Fig. S6F-G). We calculated the penetrance of EnVs formation when we blocked JNK and overexpressed *Idgf3* (*Idgf3-OE*). In *Ras^{V12}* SGs we observed EnVs in 100 % of the glands, an effect that was strongly blocked in *JNK^{DN};;Ras^{V12}* (Fig. 6 F-G, quantified in K). Blocking JNK and overexpressing *Idgf3* in *Ras^{V12}* strongly reverted the *JNK^{DN};;Ras^{V12}* phenotype - a lumen could not be detected, and around 98% of the glands contained enlarged endosomes (Fig. 6F,I, quantified in K). Overexpression of Idgf3 alone did not result in EnV formation (Fig. 6B-E). In conclusion, the data suggest that Idgf3 acts downstream of JNK and through formation of EnV's which disrupts luminal integrity.

αSpectrin has been shown to act downstream of Rac1 (Lee and Thomas 2011). With our *Bx* driver, we could reproduce this epistasis. *Rac1-OE* was sufficient to interfere with apicobasal polarity without forming detectable EnVs, and this phenotype was reverted in *Rac1-OE;αSpec-KD* (Fig. S6K-O). In order to find out whether the same epistasis takes place between Rac1 and αSpectrin in *Ras^{V12}* glands, we investigated luminal integrity. In *Rac1-OE;αSpec-KD/Ras^{V12}*, partial restoration of the lumen was observed, indicating that apicobasal polarity improved (Fig. S6 L, P-Q). Moreover, *Pak-KD;Ras^{V12}* showed lower αSpectrin levels in comparison to *Ras^{V12}* (Fig. S6S,W quantified in Y). This suggests that αSpectrin acts downstream of Rac1 in *Ras^{V12}* glands.

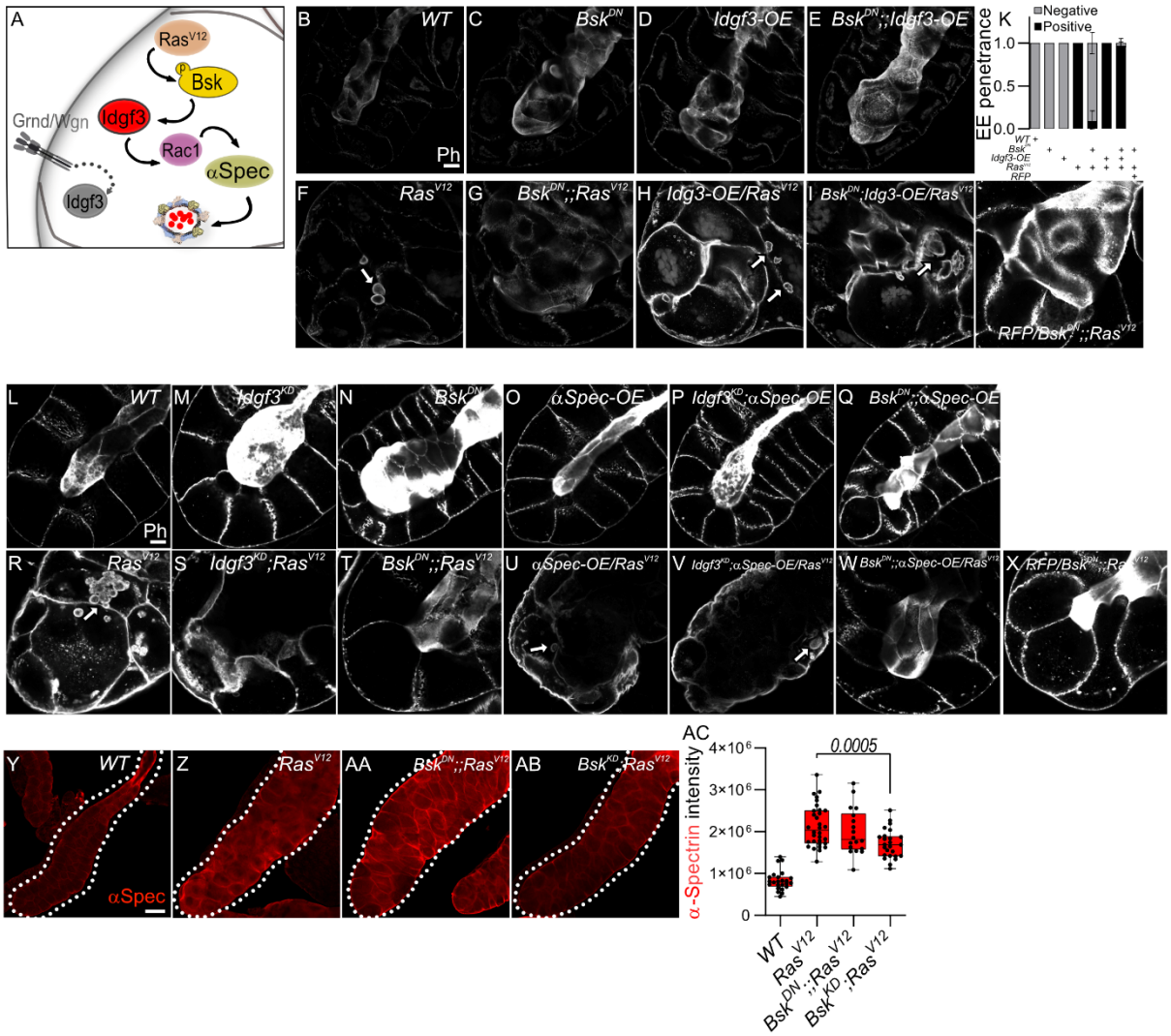

Figure 6 Idgf3 promotes activation of Rac1 and loss of cell polarity through αSpectrin

(A) Idgf3 promotes formation of EnVs, upstream of Rac1.

(B-J) Phalloidin staining showing epistasis of EnVs formation in which Idgf3 acts downstream of JNK.

(K) EnVs penetrance quantification showing a strong induction of EnVs in *JNK^{DN};;Idgf3-OE/Ras^{V12}* glands.

(L-X) Epistatic analysis between Idgf3 and αSpectrin. Phalloidin staining showing EnVs presence in *Idgf3-KD;αSpec-OE/ Ras^{V12}*.

(Y-AB) αSpectrin levels were reduced in *JNK-KD;Ras^{V12}* in comparison to *Ras^{V12}* but not in *JNK^{DN};Ras^{V12}* glands, quantified in (AC).

Scale bars in (B-J and L-X) represent 20 μm and (Y-AB) 100 μm. Barplot in (K) represent 3 independent replicas with at least 10 SG pairs, summarized a mean ± SD. Boxplot in (AC) represent at least 19 SG pairs. Whisker length min to max, bar represent median. P-value quantified with Student's t-test.

To further dissect the epistasis between JNK-Idgf3 and Rac1-αSpectrin in *Ras^{V12}* glands, we addressed the relationship between Idgf3 and αSpectrin by addressing luminal integrity. As previously described, *Idgf3-KD;Ras^{V12}* SGs showed a partially restored lumen, an indication of an improved apicobasal polarity (Fig. 6R-S).Moreover, the glands displayed lower αSpectrin

levels in comparison to *Ras^{V12}* (Fig.4R-S). Conversely, *Idgf3-KD;αSpec-OE/ Ras^{V12}* glands displayed weak F-actin staining and rounded cells containing EnVs (Fig. 6R,V). This suggests that αSpec acts downstream of Idgf3. In contrast, *JNK^{DN};;αSpec-OE/ Ras^{V12}* SGs did not lose their polarity shown by F-actin staining, indicating that αSpec acts upstream of JNK, a phenotype independent of the dilution of the driver (Fig. 6R,W-X).

The unexpected epistatic relationship between Idgf3 and αSpectrin downstream of JNK (Fig. 6L-X) led us to speculate whether the levels of JNK might play a role. Indeed, staining the gland for αSpectrin showed no significant difference in the intensity between *Ras^{V12}* and *JNK^{DN};;Ras^{V12}* (Fig. S6R-V, quantified in W). Conversely, when we used *JNK-KD* to diminish JNK levels, the levels of αSpectrin were also reduced (in *JNK-KD;Ras^{V12})* when compared to *Ras^{V12}* alone (Fig. 6Y-AB, quantified in AC). These data indicate a complex interaction between JNK levels and disruption of apicobasal polarity mediated by Idgf3 via αSpectrin. In summary, Idgf3 promotes endosome formation via increased levels of αSpec, and as a result, the SGs lose apicobasal polarity and overgrow.

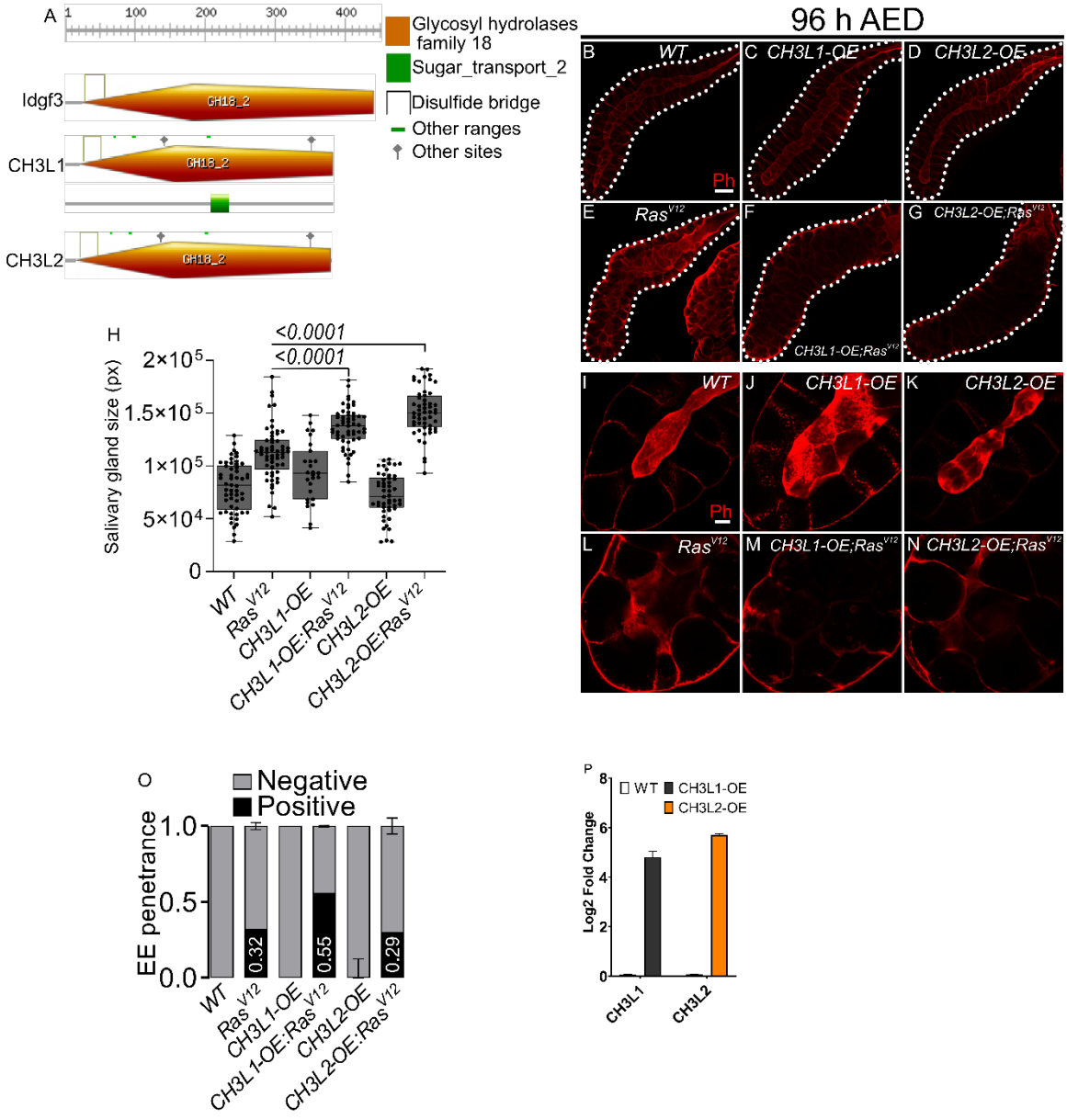

Figure 7 Human Chitinase-like proteins similarly to Idgf3 promotes EnVs formation

(A) Comparison of Idgf3, CH3L1 and CH3L2 protein motifs (https://prosite.expasy.org).
(B-G) Representative images of phalloidin staining used for size quantification.
(H) SG size quantification showing an increase in tissue size in *CH3L1-OE;Ras^{V12}* and *CH3L2-OE;Ras^{V12}* SG compared to *Ras^{V12}* alone.
(I-N) Phalloidin staining depicting disrupted lumen integrity in *Ras^{V12}* glands.
(O) EnVs penetrance quantification showing an induction of EnVs in *CH3L1-OE;Ras^{V12}* glands.
(P) qPCR confirmation of CH3L1 and CH3L2 expression in SG.
Scale bars in (B-G) represent 100 μm and (I-N) 20 μm. Boxplot in (H) represent at least 19 SG pairs. Whisker length min to max, bar represent median. P-value quantified with Student's t-test. Barplot in (O) represent 3 independent replicas with at least 10 SG pairs, summarized as

mean ± SD. Column chart in (P) represent 4 independent replicas with at least 10 SG pairs, summarized as mean ± SD.

Human CLP members enhance dysplasia in *Drosophila* SGs.

Finally, we also wished to determine whether the tumor-modulating effects we had observed for *Drosophila* Idgf3 also applied to human CLP members. For this we expressed two human *CLPs* (*Ch3L1* or *Ykl-40*; 29% AA identity and *Ch3L2* or *Ykl-39*; 26% AA identity, Fig. 7A) in SGs, both on their own and in combination with Ras^{V12}. Similar to Idgf3, both CLPs enhanced the hypertrophy observed in Ras^{V12} SGs (Fig. 7 B-K and O). Additionally, *Ch3L1* enhanced the prevalence of EnVs in the Ras mutant background. Taken together this means that the tumor-promoting effect of CLPs is conserved between *Drosophila* and humans and may affect different phenotypes of dysplasia depending on the CLP under study.

Discussion

The levels of Chitinase-like proteins (CLPs) are elevated during a wide range of inflammatory regenerative and neoplastic disorders. Their physiological function has been more elusive but includes regenerative processes such as the restoration of cell integrity after oxidative damage (Lee, Da Silva et al. 2011). Induction of CLPs has been associated with cancer development with poor prognosis (reviewed in (Zhao, Su et al. 2020)), but their role in ductal tumors is understudied. We used *Drosophila* as a tumor model to dissect CLP (*Idgf3*) function genetically in a highly secretory ductal organ, the salivary glands. We show that Idgf3 promotes tumor overgrowth through the disruption of cell polarity. The tissue and cell-autonomous induction of *Idgf3* disrupts cell organization and leads to the formation of enlarged endosome vesicles (EnVs) that accumulate in the cytoplasm. Genetically, *Idgf3* is induced via a pro-tumorigenic JNK and ROS signaling feedback loop. Consequently, Idgf3 disrupts the organization of the spectrin-based membrane skeleton (SBMS) through formation of EnVs via activation of Rac1. Significantly, KD of *Idgf3* inhibits overgrowth, restores cell polarity, and reduces ECM size and nuclear volume through blockage of EnV formation.

Our identification of a contribution of JNK sigaling and both extra- and intracellular ROS to dysplasia is in line with previous findings from other *Drosophila* tumor models (Fogarty and Bergmann 2017). Similarly, we observe an amplification loop between ROS and JNK signaling, which augments the dysplastic phenotype ((Krautz, Khalili et al. 2020)). Several studies have demonstrated that activation of JNK signaling in mammals promotes the progression of ductal tumors (Yeh, Hou et al. 2006, Tang, Sun et al. 2013, Insua-Rodriguez, Pein et al. 2018). Here we identify Idgf3 as an additional component that feeds into JNK signaling, possibly in a concentration dependent manner (Fig. 6). Ultimately in Ras^{V12}-expressing SGs, this leads to the formation of EnVs involving Spectrins. Members of the Spectrin family have a supporting role in providing cellular architecture through interaction with phospholipids and actively promoting polymerization of F-actin (Juliano, Kimelberg et al. 1971, Pinder, Bray et al. 1975, Hardy and Schrier 1978). Moreover, the secretory activity of ductal organs has been shown to be facilitated by Spectrins (Lattner, Leng et al. 2019).

During *Drosophila* development and under physiological conditions, the pathway that involves Spectrins, Rac1 and Pak1 has been shown to be required for the maintenance of cell polarity while when deregulated, it leads to the formation of enlarged vesicles similar to the EnVs(Lee and Thomas 2011). Thus our results provide a possible link between the observed induction of CLPs in a range of tumors and the effects of Spectrins and their deregulation (Ackermann and Brieger 2019, Yang, Yang et al. 2021). In addition to the genetic interaction, previous work suggests a mechanical link between spectrins via a Spectrin binding protein Hssh3bp1 (Human spectrin Src homology domain binding protein1; (Ziemnicka-Kotula, Xu et al. 1998)), the loss of which has been associated with prostatic tumors (Macoska, Xu et al. 2001). Hhh3bp1 may influence tumor progression possibly through interaction with tyrosine kinases such as Abelson tyrosine kinase (Macoska, Xu et al. 2001). Interestingly Hhh3bp1 is a marker and possible regulator of macropinocytosis, a recycling pathway that is known to be hijacked by Ras-transformed tumor cells to acquire nutrients (Recouvreux and Commisso 2017) and also leads to the formation of large intracellular vesicles. In favour of this hypothesis, macropinocytosis has been found to depend on Rac1/Pak1 signaling, although the resulting vesicles are usually smaller (0.2-5 micrometers) than EnVs (Maxson, Sarantis et al. 2021). We find that - like macropinocytosis - EnV-formation depends on the activity of growth factor receptors (Recouvreux and Commisso 2017), in this case Idgf3, much in line with its original description as an *in vitro* mediator of insulin signaling (Kawamura, Shibata et al. 1999). *In vivo*, under normal conditions, Idgf3 is required for proper formation of chitin-containing structures, wound healing and cellular integrity (Pesch, Riedel et al. 2016). Thus, under these circumstances Idgf3 may help to preserve SG integrity including the epithelial character of SG cells upstream of spectrins. Conversely, in a non-physiological setting such as upon overexpression of Ras^{V12}, this mechanism is overwhelmed leading to the breakdown of homeostasis, loss of cell polarity and the gland lumen, loss of secretory activivity and the formation of EnVs larger than macropinocytic vesicles. In a mammalian setting, the associated phenotypes such as disruption of cellular polarity and reorganization of the ECM provide targets for therapeutic treatments (Insua-Rodriguez, Pein et al. 2018). Depending on the tissue environment, CLP's may have various roles in a context-dependent manner. Overexpression of *Idgf3* alone is not sufficient for the loss of cell polarity, growth, and fibrosis. Collectively, this suggests a tumor-specific phenotype for Idgf3 (Fig. 6B-J), similar to mammalian CLPs (reviewed in (Zhao, Su et al. 2020)). In support for a phylogenetically conserved contribution of CLPs to tumor progression, we were able to recapitulate SG hypertrophy and EnV formation when we expressed two human CLPs in Ras^{V12} SGs. Whether the differences we observe between the two human CLPs is due to their different structure awaits further work. Similarly, due to their pleiotropic effects, further investigation of the role of CLPs will be required to dissect their molecular function in a given tissue and to ultimately design tumor-specific treatments (Kzhyshkowska, Larionova et al. 2019).

Taken together our findings provide new insight into the loss of tissue integrity in a neoplastic tumor model and provide targets to test how developmentally and physiologically important deregulated mechanisms contribute to tumor progession in certain forms of cancer.

Acknowledgments

We would like to thank Chris Molenaar, Roger Karlsson, Stina Höglund and the Imaging facility at Stockholm University for support with all aspects of microscopy. We would also like to thank Vasilios Tsarouhas for his critical feedback. This work was supported by grants from the Swedish Cancer Foundation (CAN 2015-546), the Wenner-Gren Foundation (UPD2020-0094 and UPD2021-0095 to MK) and the Swedish Research Council (VR 2016-04077 and VR 2021-04841).

References

Ackermann, A. and A. Brieger (2019). "The Role of Nonerythroid Spectrin alphaII in Cancer." J Oncol **2019**: 7079604.

Aggarwal, V., H. S. Tuli, A. Varol, F. Thakral, M. B. Yerer, K. Sak, M. Varol, A. Jain, M. A. Khan and G. Sethi (2019). "Role of Reactive Oxygen Species in Cancer Progression: Molecular Mechanisms and Recent Advancements." Biomolecules **9**(11).

Andersen, D. S., J. Colombani, V. Palmerini, K. Chakrabandhu, E. Boone, M. Rothlisberger, J. Toggweiler, K. Basler, M. Mapelli, A. O. Hueber and P. Leopold (2015). "The Drosophila TNF receptor Grindelwald couples loss of cell polarity and neoplastic growth." Nature **522**(7557): 482-486.

Archibald, A., C. Mihai, I. G. Macara and L. McCaffrey (2015). "Oncogenic suppression of apoptosis uncovers a Rac1/JNK proliferation pathway activated by loss of Par3." Oncogene **34**(24): 3199-3206.

Asano, K., M. Miwa, K. Miwa, R. Hanayama, H. Nagase, S. Nagata and M. Tanaka (2004). "Masking of phosphatidylserine inhibits apoptotic cell engulfment and induces autoantibody production in mice." J Exp Med **200**(4): 459-467.

Baek, S. H., Y. C. Kwon, H. Lee and K. M. Choe (2010). "Rho-family small GTPases are required for cell polarization and directional sensing in Drosophila wound healing." Biochem Biophys Res Commun **394**(3): 488-492.

Bartlett, B. J., P. Isakson, J. Lewerenz, H. Sanchez, R. W. Kotzebue, R. C. Cumming, G. L. Harris, I. P. Nezis, D. R. Schubert, A. Simonsen and K. D. Finley (2011). "p62, Ref(2)P and ubiquitinated proteins are conserved markers of neuronal aging, aggregate formation and progressive autophagic defects." Autophagy **7**(6): 572-583.

Bennett, V. and A. J. Baines (2001). "Spectrin and ankyrin-based pathways: metazoan inventions for integrating cells into tissues." Physiol Rev **81**(3): 1353-1392.

Brumby, A. M. and H. E. Richardson (2003). "scribble mutants cooperate with oncogenic Ras or Notch to cause neoplastic overgrowth in Drosophila." EMBO J **22**(21): 5769-5779.

Ciapponi, L., D. B. Jackson, M. Mlodzik and D. Bohmann (2001). "Drosophila Fos mediates ERK and JNK signals via distinct phosphorylation sites." Genes Dev **15**(12): 1540-1553.

Diwanji, N. and A. Bergmann (2017). "The beneficial role of extracellular reactive oxygen species in apoptosis-induced compensatory proliferation." Fly (Austin) **11**(1): 46-52.

Faria, C. C. and R. S. Fortunato (2020). "The role of dual oxidases in physiology and cancer." Genet Mol Biol **43**(1 suppl. 1): e20190096.

Fernandez-Medarde, A., J. De Las Rivas and E. Santos (2021). "40 Years of RAS-A Historic Overview." Genes (Basel) **12**(5).

Fletcher, G. C., A. Elbediwy, I. Khanal, P. S. Ribeiro, N. Tapon and B. J. Thompson (2015). "The Spectrin cytoskeleton regulates the Hippo signalling pathway." EMBO J **34**(7): 940-954.

Fogarty, C. E. and A. Bergmann (2017). "Killers creating new life: caspases drive apoptosis-induced proliferation in tissue repair and disease." Cell Death Differ **24**(8): 1390-1400.

Hardy, B. and S. L. Schrier (1978). "The role of spectrin in erythrocyte ghost endocytosis." Biochem Biophys Res Commun **81**(4): 1153-1161.

Igaki, T., R. A. Pagliarini and T. Xu (2006). "Loss of cell polarity drives tumor growth and invasion through JNK activation in Drosophila." Curr Biol **16**(11): 1139-1146.

Insua-Rodriguez, J., M. Pein, T. Hongu, J. Meier, A. Descot, C. M. Lowy, E. De Braekeleer, H. P. Sinn, S. Spaich, M. Sutterlin, A. Schneeweiss and T. Oskarsson (2018). "Stress signaling in breast cancer cells induces matrix components that promote chemoresistant metastasis." EMBO Mol Med **10**(10).

Johansen, J. S., B. V. Jensen, A. Roslind, D. Nielsen and P. A. Price (2006). "Serum YKL-40, a new prognostic biomarker in cancer patients?" Cancer Epidemiol Biomarkers Prev **15**(2): 194-202.

Juliano, R. L., H. K. Kimelberg and D. Papahadjopoulos (1971). "Synergistic effects of a membrane protein (spectrin) and Ca 2+ on the Na + permeability of phospholipid vesicles." Biochim Biophys Acta **241**(3): 894-905.

Kanda, H., T. Igaki, H. Kanuka, T. Yagi and M. Miura (2002). "Wengen, a member of the Drosophila tumor necrosis factor receptor superfamily, is required for Eiger signaling." J Biol Chem **277**(32): 28372-28375.

Karlsson, C., A. M. Korayem, C. Scherfer, O. Loseva, M. S. Dushay and U. Theopold (2004). "Proteomic analysis of the Drosophila larval hemolymph clot." J Biol Chem **279**(50): 52033-52041.

Kawamura, K., T. Shibata, O. Saget, D. Peel and P. J. Bryant (1999). "A new family of growth factors produced by the fat body and active on Drosophila imaginal disc cells." Development **126**(2): 211-219.

Khalili, D., C. Kalcher, S. Baumgartner and U. Theopold (2021). "Anti-Fibrotic Activity of an Antimicrobial Peptide in a Drosophila Model." J Innate Immun: 1-15.

Khalili, D., C. Kalcher, S. Baumgartner and U. Theopold (2021). "Anti-Fibrotic Activity of an Antimicrobial Peptide in a Drosophila Model." J Innate Immun **13**(6): 376-390.

Kirkpatrick, R. B., R. E. Matico, D. E. McNulty, J. E. Strickler and M. Rosenberg (1995). "An abundantly secreted glycoprotein from Drosophila melanogaster is related to mammalian secretory proteins produced in rheumatoid tissues and by activated macrophages." Gene **153**(2): 147-154.

Krautz, R., D. Khalili and U. Theopold (2020). "Tissue-autonomous immune response regulates stress signalling during hypertrophy." Elife **9**.

Kucerova, L., O. I. Kubrak, J. M. Bengtsson, H. Strnad, S. Nylin, U. Theopold and D. R. Nassel (2016). "Slowed aging during reproductive dormancy is reflected in genome-wide transcriptome changes in Drosophila melanogaster." BMC Genomics **17**(1): 50.

Kzhyshkowska, J., I. Larionova and T. Liu (2019). "YKL-39 as a Potential New Target for Anti-Angiogenic Therapy in Cancer." Front Immunol **10**: 2930.

Lattner, J., W. Leng, E. Knust, M. Brankatschk and D. Flores-Benitez (2019). "Crumbs organizes the transport machinery by regulating apical levels of PI(4,5)P2 in Drosophila." Elife **8**.

Lee, C. G., C. A. Da Silva, C. S. Dela Cruz, F. Ahangari, B. Ma, M. J. Kang, C. H. He, S. Takyar and J. A. Elias (2011). "Role of chitin and chitinase/chitinase-like proteins in inflammation, tissue remodeling, and injury." Annual review of physiology **73**: 479-501.

Lee, S. K. and G. H. Thomas (2011). "Rac1 modulation of the apical domain is negatively regulated by beta (Heavy)-spectrin." Mech Dev **128**(1-2): 116-128.

Macoska, J. A., J. Xu, D. Ziemnicka, T. S. Schwab, M. A. Rubin and L. Kotula (2001). "Loss of expression of human spectrin src homology domain binding protein 1 is associated with 10p loss in human prostatic adenocarcinoma." Neoplasia **3**(2): 99-104.

Maxson, M. E., H. Sarantis, A. Volchuk, J. H. Brumell and S. Grinstein (2021). "Rab5 regulates macropinocytosis by recruiting the inositol 5-phosphatases OCRL and Inpp5b that hydrolyse PtdIns(4,5)P2." J Cell Sci **134**(7).

Morera, E., S. S. Steinhauser, Z. Budkova, S. Ingthorsson, J. Kricker, A. Krueger, G. A. Traustadottir and T. Gudjonsson (2019). "YKL-40/CHI3L1 facilitates migration and invasion in HER2 overexpressing breast epithelial progenitor cells and generates a niche for capillary-like network formation." In Vitro Cell Dev Biol Anim **55**(10): 838-853.

Pagliarini, R. A. and T. Xu (2003). "A genetic screen in Drosophila for metastatic behavior." Science **302**(5648): 1227-1231.

Palmerini, V., S. Monzani, Q. Laurichesse, R. Loudhaief, S. Mari, V. Cecatiello, V. Olieric, S. Pasqualato, J. Colombani, D. S. Andersen and M. Mapelli (2021). "Drosophila TNFRs Grindelwald and Wengen bind Eiger with different affinities and promote distinct cellular functions." Nat Commun **12**(1): 2070.

Park, K. R., H. M. Yun, K. Yoo, Y. W. Ham, S. B. Han and J. T. Hong (2020). "Chitinase 3 like 1 suppresses the stability and activity of p53 to promote lung tumorigenesis." Cell Commun Signal **18**(1): 5.

Perez, E., J. L. Lindblad and A. Bergmann (2017). "Tumor-promoting function of apoptotic caspases by an amplification loop involving ROS, macrophages and JNK in Drosophila." Elife **6**.

Perkins, K. K., G. M. Dailey and R. Tjian (1988). "Novel Jun- and Fos-related proteins in Drosophila are functionally homologous to enhancer factor AP-1." EMBO J **7**(13): 4265-4273.

Pesch, Y. Y., D. Riedel, K. R. Patil, G. Loch and M. Behr (2016). "Chitinases and Imaginal disc growth factors organize the extracellular matrix formation at barrier tissues in insects." Sci Rep **6**: 18340.

Pinder, J. C., D. Bray and W. B. Gratzer (1975). "Actin polymerisation induced by spectrin." Nature **258**(5537): 765-766.

Pinho, A. V., L. Chantrill and I. Rooman (2014). "Chronic pancreatitis: a path to pancreatic cancer." Cancer Lett **345**(2): 203-209.

Recouvreux, M. V. and C. Commisso (2017). "Macropinocytosis: A Metabolic Adaptation to Nutrient Stress in Cancer." Front Endocrinol (Lausanne) **8**: 261.

Roslind, A. and J. S. Johansen (2009). "YKL-40: a novel marker shared by chronic inflammation and oncogenic transformation." Methods Mol Biol **511**: 159-184.

Shao, R., K. Hamel, L. Petersen, Q. J. Cao, R. B. Arenas, C. Bigelow, B. Bentley and W. Yan (2009). "YKL-40, a secreted glycoprotein, promotes tumor angiogenesis." Oncogene **28**(50): 4456-4468.

Tang, H., Y. Sun, Z. Shi, H. Huang, Z. Fang, J. Chen, Q. Xiu and B. Li (2013). "YKL-40 induces IL-8 expression from bronchial epithelium via MAPK (JNK and ERK) and NF-kappaB pathways, causing bronchial smooth muscle proliferation and migration." J Immunol **190**(1): 438-446.

Tjota, M., S. K. Lee, J. Wu, J. A. Williams, M. R. Khanna and G. H. Thomas (2011). "Annexin B9 binds to beta(H)-spectrin and is required for multivesicular body function in Drosophila." J Cell Sci **124**(Pt 17): 2914-2926.

Tran, D. T. and K. G. Ten Hagen (2017). "Real-time insights into regulated exocytosis." J Cell Sci **130**(8): 1355-1363.

Uhlen, M., C. Zhang, S. Lee, E. Sjostedt, L. Fagerberg, G. Bidkhori, R. Benfeitas, M. Arif, Z. Liu, F. Edfors, K. Sanli, K. von Feilitzen, P. Oksvold, E. Lundberg, S. Hober, P. Nilsson, J. Mattsson, J. M. Schwenk, H. Brunnstrom, B. Glimelius, T. Sjoblom, P. H. Edqvist, D. Djureinovic, P. Micke, C. Lindskog, A. Mardinoglu and F. Ponten (2017). "A pathology atlas of the human cancer transcriptome." Science **357**(6352).

Wertheimer, E., A. Gutierrez-Uzquiza, C. Rosemblit, C. Lopez-Haber, M. S. Sosa and M. G. Kazanietz (2012). "Rac signaling in breast cancer: a tale of GEFs and GAPs." Cell Signal **24**(2): 353-362.

Williams, S. T., A. N. Smith, C. D. Cianci, J. S. Morrow and T. L. Brown (2003). "Identification of the primary caspase 3 cleavage site in alpha II-spectrin during apoptosis." Apoptosis **8**(4): 353-361.

Wu, C., C. Chen, J. Dai, F. Zhang, Y. Chen, W. Li, J. C. Pastor-Pareja and L. Xue (2015). "Toll pathway modulates TNF-induced JNK-dependent cell death in Drosophila." Open Biol **5**(7): 140171.

Yadav, S. and I. Eleftherianos (2018). "The Imaginal Disc Growth Factors 2 and 3 participate in the Drosophila response to nematode infection." Parasite Immunol **40**(10): e12581.

Yang, P., Y. Yang, P. Sun, Y. Tian, F. Gao, C. Wang, T. Zong, M. Li, Y. Zhang, T. Yu and Z. Jiang (2021). "betaII spectrin (SPTBN1): biological function and clinical potential in cancer and other diseases." Int J Biol Sci **17**(1): 32-49.

Yeh, Y. T., M. F. Hou, Y. F. Chung, Y. J. Chen, S. F. Yang, D. C. Chen, J. H. Su and S. S. Yuan (2006). "Decreased expression of phosphorylated JNK in breast infiltrating ductal carcinoma is associated with a better overall survival." Int J Cancer **118**(11): 2678-2684.

Zeke, A., M. Misheva, A. Remenyi and M. A. Bogoyevitch (2016). "JNK Signaling: Regulation and Functions Based on Complex Protein-Protein Partnerships." Microbiol Mol Biol Rev **80**(3): 793-835.

Zhao, T., Z. Su, Y. Li, X. Zhang and Q. You (2020). "Chitinase-3 like-protein-1 function and its role in diseases." Signal Transduct Target Ther **5**(1): 201.

Zhu, M., T. Xin, S. Weng, Y. Gao, Y. Zhang, Q. Li and M. Li (2010). "Activation of JNK signaling links lgl mutations to disruption of the cell polarity and epithelial organization in Drosophila imaginal discs." Cell Res **20**(2): 242-245.

Ziemnicka-Kotula, D., J. Xu, H. Gu, A. Potempska, K. S. Kim, E. C. Jenkins, E. Trenkner and L. Kotula (1998). "Identification of a candidate human spectrin Src homology 3 domain-binding protein suggests a general mechanism of association of tyrosine kinases with the spectrin-based membrane skeleton." J Biol Chem **273**(22): 13681-13692.